

# Simple atom interferometer in a double-well potential

Karol Gietka and Jan Chwedeńczuk  
*Faculty of Physics, University of Warsaw,  
ul. Hoża 69, 00-681 Warsaw, Poland*

We present a detailed study of an atom interferometer which can be realized in a double-well potential. We assume that the interferometric phase is imprinted in the presence of coherent tunneling between the wells. We calculate the ultimate bounds for the estimation sensitivity and show how they relate to the precision of the Mach-Zehnder interferometer. The interferometer presented here allows for sub shot-noise sensitivity when fed with the spin-squeezed states with reduced either the relative population imbalance or the relative phase. We also calculate the precision of the estimation from the population imbalance and show that it overcomes the shot-noise level when the entangled squeezed-states are used at the input.

PACS numbers: 37.25.+k, 03.75.-b, 03.75.Lm

## I. INTRODUCTION

The key objective of quantum interferometry is to enhance the estimation precision  $\Delta\theta$  of an unknown parameter  $\theta$  using non-classical correlations as a resource. The reference value  $\Delta\theta_{\text{SN}} = \frac{1}{\sqrt{m}} \frac{1}{\sqrt{N}}$  is called the shot-noise limit (SNL), with  $N$  being the number of particles passing through the interferometer and  $m$  being the number of measurement repetitions. The SNL is the best achievable sensitivity in the classical two-mode interferometry. Only in the presence of useful particle entanglement, the SNL can be surpassed [1, 2] to give  $\Delta\theta < \Delta\theta_{\text{SN}}$ . Therefore, quantum interferometry can be viewed from two perspectives. From one point of view, the stress is put on the preparation of a usefully entangled quantum state which together with the estimation protocol cooperate to give  $\Delta\theta < \Delta\theta_{\text{SN}}$ . From the other point of view, interferometry is a tool for detecting quantum correlations in many-body systems. In this case, the value of  $\Delta\theta$  is treated as a probe of the particle entanglement.

The  $\Delta\theta$  can be evaluated using the Cramer-Rao lower bound (CRLB) [3]. This important theorem links the sensitivity with the Fisher information

$$\Delta\theta \geq \frac{1}{\sqrt{m}} \frac{1}{\sqrt{F}}. \quad (1)$$

The value of  $F$  depends on all the three steps of the interferometric sequence: the preparation of the state which enters the device, the type of the interferometric transformation, and the measurement performed at the output to obtain  $\theta$ . According to the definition of the SNL,  $F > N$  signals the particle entanglement [2]. However, in most experimental situations, it is very difficult to directly measure the value of  $F$ . The solution to this problem is to replace the Fisher information in Eq. (1) with some other physical quantity which is more accessible in the laboratory. However, this new quantity sets a weaker constraint than the CRLB (1).

This approach is illustrated by a broad use of the spin-squeezing parameter  $\xi_n^2$  [4, 5]. It is proportional to the

fluctuations of the number of particles between the two modes divided by the visibility of the one-body fringes. Spin-squeezed states ( $\xi_n^2 < 1$ ) are particle-entangled and potentially useful for quantum metrology. Recently, the spin-squeezing has been generated in two-mode quantum systems [6–12]. A similar technique to detect the non-classical correlations was used in a collection of atoms scattered from a single Bose-Einstein condensate in the spin-changing collisions [13].

A usefully entangled quantum state passes through a metrological device, for example, the Mach-Zehnder interferometer (MZI) which is realized in three steps. First, the two-mode state goes through a beam splitter, then a phase  $\theta$  is imprinted on one of the arms, and finally another beam splitter mixes the modes to yield an interferometric signal. The MZI can benefit from the quantum correlations present in the spin-squeezed state to provide the sensitivity  $\Delta\theta$  below the SNL [2, 14]. Another type of an interferometric sequence is based on the Bloch oscillations of a gas in a double- (or many-) well potential [15–22]. In this scenario, the external force drives the coherent oscillations between the sites of the periodic potential. Therefore, in contrast to the MZI, the mode mixing occurs simultaneously with the phase imprint.

In this work, we study in detail a performance of an interferometer where the phase imprint is accompanied by the tunneling of the gas between the two sites of the trapping potential. In Section II, we introduce a simple model for the two-mode system of ultra-cold bosons trapped in a double-well potential. We determine the evolution operator and present the family of input states convenient for our analysis. In Section III, using the notion of the quantum Fisher information, we calculate the ultimate bounds for the precision of such a double-well interferometer. In Section IV, we calculate the precision for a particular choice of the estimation protocol and compare these results to the ultimate bounds. The conclusions are contained in Section V. This work is an extension of a previous study [23] where the outline of the theory of such an interferometer was presented.

## II. THE MODEL

We consider a collection of  $N$  non-interacting bosons trapped in a symmetric double-well potential  $V_{\text{dw}}(x)$ . The system is driven into the oscillations between the two wells due to the presence of an external force with a potential  $V(x)$ . The objective of the following inquiry is to examine how, and with what precision, the strength of  $V(x)$  can be determined. To accomplish this task, we employ the two-mode approximation where the field operator reads

$$\hat{\Psi}(x) = \psi_a(x)\hat{a} + \psi_b(x)\hat{b}. \quad (2)$$

Here  $\hat{a}/\hat{b}$  annihilates a boson in a left/right potential well, and  $\psi_{a/b}(x)$  is a corresponding spatial wave-packet. The Hamiltonian of the system is

$$\hat{H} = \int dx \hat{\Psi}^\dagger(x) \left[ -\frac{\hbar^2}{2M} \frac{\partial^2}{\partial x^2} + V_{\text{dw}}(x) + V(x) \right] \hat{\Psi}(x), \quad (3)$$

where  $M$  is the atomic mass. We employ the definition of the Josephson energy  $E_J$  and the detuning  $\delta$ , i.e.,

$$E_J = 2 \int dx \psi_a^*(x) \left[ -\frac{\hbar^2}{2M} \frac{\partial^2}{\partial x^2} + V_{\text{dw}}(x) \right] \psi_b(x) \quad (4a)$$

$$\delta = \int dx (|\psi_a(x)|^2 - |\psi_b(x)|^2) V(x) \quad (4b)$$

to obtain that, up to the constant terms, the Hamiltonian (3) can be expressed in a compact form

$$\hat{H} = -E_J \hat{J}_x + \delta \hat{J}_z. \quad (5)$$

The  $\hat{J}_x$  and  $\hat{J}_z$  angular momentum operators which appear above, together with the  $y$ -component, read

$$\hat{J}_x = \frac{1}{2}(\hat{a}^\dagger \hat{b} + \hat{a} \hat{b}^\dagger) \quad (6a)$$

$$\hat{J}_y = \frac{1}{2i}(\hat{a}^\dagger \hat{b} - \hat{a} \hat{b}^\dagger) \quad (6b)$$

$$\hat{J}_z = \frac{1}{2}(\hat{a}^\dagger \hat{a} - \hat{b}^\dagger \hat{b}). \quad (6c)$$

These operators form a Lie algebra  $[\hat{J}_k, \hat{J}_l] = i\epsilon_{klm}\hat{J}_m$ . The Hamiltonian (5) generates the unitary evolution

$$\hat{U} = \exp \left[ i\varphi(\hat{J}_x - \epsilon \hat{J}_z) \right]. \quad (7)$$

Here  $\epsilon = \delta/E_J$  is the ratio of the detuning to the Josephson energy, while  $\varphi = E_J t/\hbar$  is the phase acquired through bare Josephson oscillations.

To simplify the further analysis, we assume that the initial state which undergoes the evolution (7) is pure

$$|\psi\rangle = \sum_{n=0}^N C_n |n, N-n\rangle \quad \text{with} \quad \sum_{n=0}^N |C_n|^2 = 1. \quad (8)$$

Depending on the coefficients  $C_n$ ,  $|\psi\rangle$  is either separable or entangled. Since this initial state is prepared in the

absence of the perturbing potential  $V(x)$ , it is reasonable to assume that it is path-symmetric, i.e.,  $C_n = C_{N-n}$ . This symmetry vastly simplifies the following discussion through the set of algebraic relations

$$\langle \hat{J}_y \rangle = \langle \hat{J}_z \rangle = \langle \hat{J}_x \hat{J}_y \rangle = \langle \hat{J}_x \hat{J}_z \rangle = \langle \hat{J}_y \hat{J}_z \rangle = 0. \quad (9)$$

The Hamiltonian (5) leads to various types of interferometric schemes depending on the ratio of the Josephson energy to the detuning  $\delta$ . One limiting case is when tunneling is fully suppressed during the action of the external force, i.e.,  $\epsilon \rightarrow \infty$ . In such a case, the interferometric transformation consists of a bare phase-imprint because the evolution operator (7) simplifies to

$$\hat{U}_{\text{ph}} = e^{-i\theta \hat{J}_z}, \quad (10)$$

where  $\theta = \delta t/\hbar$ . To obtain some  $\theta$ -dependent signal, additional mode-mixing manipulation is necessary. Usually, two distinct scenarios are considered to accomplish this task. In the first one, the phase imprint (10) is preceded and followed by a pair of beam-splitters, and the full cycle is the MZI with an effective evolution operator

$$\hat{U}_{\text{MZI}} = e^{-i\theta \hat{J}_y}. \quad (11)$$

Note that when the two modes represent atomic internal degrees of freedom, the beam-splitters can be realized by applying a precisely crafted rf-pulse [8, 9, 13]. However, when the modes are spatially separated, as in a double-well potential [12, 24–27], the beam-splitter is more difficult to implement. In an alternative scenario of obtaining the interferometric signal from the evolution (10), the gas is simply released from the trap. In the far-field regime, an interference pattern is formed, and  $\theta$  can be inferred from the measurements of positions of individual atoms [28], for instance, from a least-square fit of the one-body density to the acquired data. In such a case, the sub shot-noise (SSN) sensitivity can be achieved with the phase-squeezed states [28, 29]. However, to reach the Heisenberg scaling, the knowledge of the full  $N$ -body correlations is necessary [30], which for large  $N$  is practically impossible.

As underlined in the Introduction, we will analyze the interferometer performance when both the tunneling and the detuning compete at the same time. Formally, this means that  $\epsilon \lesssim 1$  and the evolution operator is given by the full expression (7) rather than the simplified (10). This type of evolution has one clear advantage over the above scenario. Namely, the modes are mixed already during the interaction of the gas with the external field, and no addition to the interferometric sequence is necessary.

It is worth to note that the Hamiltonian (5) generates the rotation of the composite spin- $\frac{N}{2}$  vector on the Bloch sphere. For such a transformation, states which give high metrological precision are those which have reduced fluctuations in the direction orthogonal to the rotation. For instance, if the interferometer rotates the

state around the  $y$ -axis—as in the MZI (11)—the useful entanglement is related to the spin-squeezing in the  $z$ -direction. It might seem that finding a usefully entangled state for the Hamiltonian (5) should be easy—one should just squeeze the state in a direction orthogonal to the vector with the Cartesian coordinates  $(-E_J, 0, \delta)$ . However, the knowledge of the direction of this vector is equivalent to the knowledge of  $\delta$  which, actually, is the parameter to be estimated. Although some adaptive methods could be used to first roughly estimate  $\delta$  and then prepare the properly entangled states, we assume that  $\delta$  remains completely unknown and the input states are typical for the two-mode atom interferometry.

Finally, note that during the evolution governed by the Hamiltonian (5), the two-body interactions are absent. This can be achieved by tuning the scattering length using the Feshbach resonances [31, 32]. Although our analysis assumes a complete lack of interactions, some residual two-body collisions might be present [17]. In a more realistic model, they should be included either perturbatively in the analytical calculation or numerically.

### III. ULTIMATE PRECISION – QUANTUM FISHER INFORMATION

In the first step, we calculate the maximal attainable precision of the estimation of  $\delta$ . With this result at hand, we will have a possibility to judge the efficiency of a simple estimation protocol. Note that usually the interferometer is characterized by its phase sensitivity  $\Delta\theta$ . Here we use  $\Delta\delta$ , which is the precision of the estimation of the sole parameter  $\delta$ . The phase sensitivity can be retrieved through a multiplication of  $\Delta\delta$  by  $t/\hbar$ , where  $t$  is the time span of the interferometric sequence.

The ultimate precision  $\Delta\delta$ , which is optimized over all the estimation strategies, is determined by the quantum Fisher information (QFI) denoted by  $F_Q$ . Its value depends on the input state  $|\psi\rangle$  and the Hamiltonian (5) which introduces the  $\delta$ -dependence into the system. For pure states, the ultimate CRLB is [33]

$$\Delta\delta \geq \frac{1}{\sqrt{m}} \frac{1}{\sqrt{F_Q}} = \frac{1}{\sqrt{m}} \frac{1}{\sqrt{4\langle(\Delta\hat{h})^2\rangle}}. \quad (12)$$

The variance  $\langle(\Delta\hat{h})^2\rangle = \langle\hat{h}^2\rangle - \langle\hat{h}\rangle^2$  is calculated for the initial state  $|\psi\rangle$ , and  $\hat{h}$  is an operator which generates the transformation

$$i\partial_\delta |\psi(\delta)\rangle = \hat{h} |\psi(\delta)\rangle. \quad (13)$$

Using  $|\psi(\delta)\rangle = \hat{U} |\psi\rangle$ , we obtain that  $\hat{h}$  is related to the evolution operator (7) by the expression

$$\hat{h} = i \frac{\partial \hat{U}}{\partial \delta} \hat{U}^\dagger. \quad (14)$$

Note that it is convenient to express the sensitivity (12) in units of  $\delta$ , i.e., to replace  $\hat{h}$  with  $\delta \cdot \hat{h}$ . Calculation of

the QFI using Equations (7), (12), and (14) is straightforward. The commutation relations of the angular momentum operators give the rescaled generator equal to

$$\hat{h} = h_x \hat{J}_x + h_y \hat{J}_y + h_z \hat{J}_z, \quad (15)$$

where the three coefficients  $h_x$ ,  $h_y$ , and  $h_z$  read

$$h_x = \frac{\epsilon^2}{\epsilon^2 + 1} \left( \frac{\sin(\varphi\sqrt{\epsilon^2 + 1})}{\sqrt{\epsilon^2 + 1}} - \varphi \right) \quad (16a)$$

$$h_y = \frac{\epsilon}{\epsilon^2 + 1} \left( 1 - \cos(\varphi\sqrt{\epsilon^2 + 1}) \right) \quad (16b)$$

$$h_z = \frac{\epsilon^3}{\epsilon^2 + 1} \left( \frac{\sin(\varphi\sqrt{\epsilon^2 + 1})}{\epsilon^2\sqrt{\epsilon^2 + 1}} + \varphi \right). \quad (16c)$$

Substituting Eq. (15) into Eq. (12), we obtain for the path-symmetric states (9)

$$F_Q = 4 \left( h_x^2 \langle(\Delta\hat{J}_x)^2\rangle + h_y^2 \langle\hat{J}_y^2\rangle + h_z^2 \langle\hat{J}_z^2\rangle \right). \quad (17)$$

Clearly, the QFI is a complicated function of the independent parameters  $\epsilon$  and  $\varphi$ , and the input state (8) by means of the two lowest moments of the angular momentum operators.

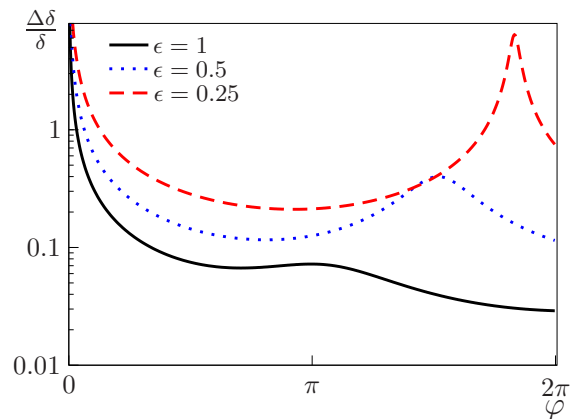


FIG. 1. (color online) The sensitivity  $\Delta\delta$  in units of  $\delta$  for a spin-coherent state with  $N = 100$  plotted as a function of  $\varphi$  for three different values of  $\epsilon = 1$  (solid black line),  $\epsilon = 0.5$  (dotted blue line), and  $\epsilon = 0.25$  (dashed red line).

We perform the systematic analysis of Eq. (17) by first fixing the input state—i.e., fixing  $\langle(\Delta\hat{J}_x)^2\rangle$ ,  $\langle\hat{J}_y^2\rangle$ , and  $\langle\hat{J}_z^2\rangle$ —and then plotting the QFI as a function of the other parameters. First, we consider a spin-coherent state

$$|\psi\rangle = \frac{1}{\sqrt{N!}} \left( \frac{\hat{a}^\dagger + \hat{b}^\dagger}{\sqrt{2}} \right)^N |0\rangle, \quad (18)$$

which gives  $\langle(\Delta\hat{J}_x)^2\rangle = 0$  and  $\langle\hat{J}_y^2\rangle = \langle\hat{J}_z^2\rangle = \frac{N}{4}$ . In such a case, the QFI scales linearly with the number of

particles (shot-noise scaling), and the sensitivity reads

$$\frac{\Delta\delta}{\delta} \geq \frac{1}{\sqrt{m}} \frac{1}{\sqrt{N}} \frac{1}{\sqrt{h_y^2 + h_z^2}}. \quad (19)$$

We plot this expression in Fig. 1 as a function of  $\varphi$  for three different values of  $\epsilon$ . For small  $\epsilon = 0.25$ , when the tunneling dominates over the detuning, oscillations are clearly visible. When  $\epsilon$  grows, the period of oscillations drops according to Eq. (16), and the sensitivity clearly improves with time. This is the result of the increasing domination of the  $\delta\hat{J}_z$  term in the Hamiltonian (5).

In the next step, we replace the spin coherent state with a spin-squeezed state which has reduced fluctuations of the relative atom number between the two modes [6–12]. Such a state is characterized with the spin-squeezing parameter [4, 5]

$$\xi_n^2 = N \frac{\langle \hat{J}_z^2 \rangle}{\langle \hat{J}_x \rangle^2}. \quad (20)$$

We numerically generate an entangled spin-squeezed state by finding the ground state of the Bose-Hubbard Hamiltonian

$$\hat{H}_{\text{bh}} = -\hat{J}_x + \frac{\alpha}{N} \hat{J}_z^2. \quad (21)$$

with  $N = 100$  particles and  $\alpha > 0$ . We take such  $\alpha$  to obtain a realistic value  $\xi_n^2 = 0.15$ . With this state, we calculate all the moments of the angular momentum operators (17) which determine the sensitivity (12). In Fig. 2, we plot the resulting sensitivity in units of  $\delta$  as a function of  $\varphi$  for the same three values of  $\epsilon$  as in Fig. 1.

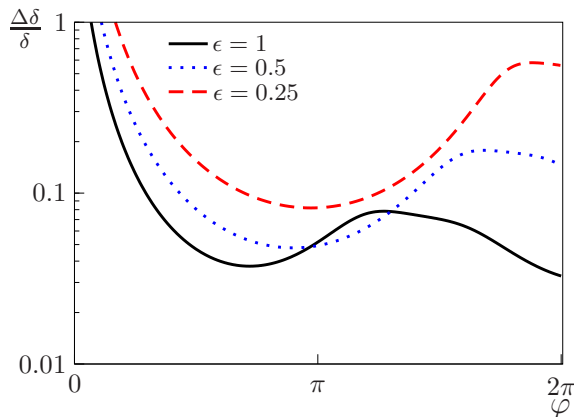


FIG. 2. (color online) The sensitivity  $\Delta\delta$  in units of  $\delta$  for a spin-squeezed state of  $N = 100$  particles with  $\xi_n^2 = 0.15$  plotted as a function of  $\varphi$  for three different values of  $\epsilon = 1$  (solid black line),  $\epsilon = 0.5$  (dotted blue line), and  $\epsilon = 0.25$  (dashed red line).

Finally, we take a phase-squeezed state, characterized by the following squeezing parameter [28, 29]

$$\xi_\phi^2 = N \frac{\langle \hat{J}_y^2 \rangle}{\langle \hat{J}_x \rangle^2}, \quad (22)$$

which we generate with the same Hamiltonian but with  $\alpha < 0$ . We take symmetrically  $\xi_\phi^2 = 0.15$  for  $N = 100$  particles and plot the analogical sensitivity in Fig. 3.

We now discuss and compare the results presented in these three figures. First, note that for large  $\epsilon$  the phase-squeezed states ( $\xi_\phi^2 < 1$ ) give better precision than the number-squeezed ( $\xi_n^2 < 1$ ). This is because in this regime the  $\delta\hat{J}_z$  term dominates in the Hamiltonian (5). For the phase-squeezed states, the terms  $\langle \hat{J}_z^2 \rangle$  in the QFI dominates over the other two parts, and the coefficient  $h_z$  grows with  $\epsilon$ . On the other hand, for the number-squeezed states, the  $\langle \hat{J}_y^2 \rangle$  dominates over the other parts of the QFI. Moreover, according to Equations (16), this term becomes more important for small  $\epsilon$ , but we still do not observe a significant improvement of the sensitivity between the results for the coherent state from Fig. 1 and the number-squeezed from Fig. 2. To explain this behav-

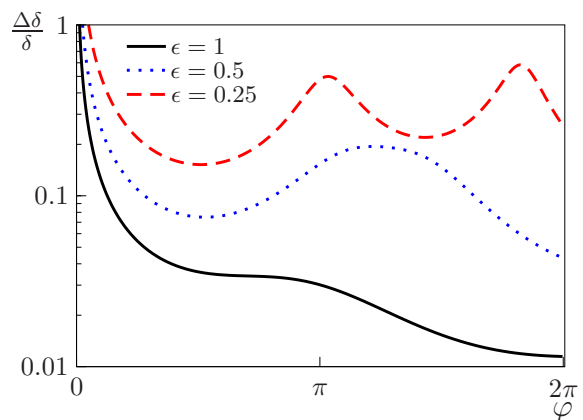


FIG. 3. (color online) The sensitivity  $\Delta\delta$  in units of  $\delta$  for a spin-squeezed state of  $N = 100$  particles with  $\xi_\phi^2 = 0.15$  plotted as a function of  $\varphi$  for three different values of  $\epsilon = 1$  (solid black line),  $\epsilon = 0.5$  (dotted blue line), and  $\epsilon = 0.25$  (dashed red line).

ior, we expand the coefficients (16) in a limit of  $\epsilon \ll 1$  and short times ( $\varphi \simeq 1$ ), and we obtain that

$$h_x \simeq \epsilon^2 (\sin \varphi - \varphi) \quad (23a)$$

$$h_y \simeq \epsilon (1 - \cos \varphi) \quad (23b)$$

$$h_z \simeq \epsilon \sin \varphi. \quad (23c)$$

Apart from the vicinity of  $\varphi = 2\pi$ , the  $h_x$  coefficient from line (23a) can be neglected compared to  $h_y$  and  $h_z$ , and the lower bound for the sensitivity reads

$$\frac{\Delta\delta}{\delta} \geq \frac{1}{\sqrt{m}} \frac{1}{2\epsilon} \frac{1}{\sqrt{(1 - \cos \varphi)^2 \langle \hat{J}_y^2 \rangle + \sin^2 \varphi \langle \hat{J}_z^2 \rangle}}. \quad (24)$$

Clearly, there is a particular point  $\varphi = \pi$  when

$$\frac{\Delta\delta}{\delta} \geq \frac{1}{\sqrt{m}} \frac{1}{2\epsilon} \frac{1}{\sqrt{4 \langle \hat{J}_y^2 \rangle}}. \quad (25)$$

This sensitivity closely resembles the ultimate bound for the MZI interferometer (11), which for pure states reads

$$\frac{\Delta\delta_{\text{MZI}}}{\delta} \geq \frac{1}{\sqrt{m}} \frac{1}{\theta} \frac{1}{\sqrt{4\langle\hat{J}_y^2\rangle}}. \quad (26)$$

However, since  $\theta = \epsilon \times \varphi$ , the MZI bound for the sensitivity is  $\varphi/2$  times better than Eq. (25). This means that the precision (26), in contrary to (25), improves over time. Nevertheless, since the expansion (23) is valid for short times, the gain from the time-scaling of Eq. (26) over (25) is of the order of  $\pi$ . Note also that the expression (25) improves for the spin-squeezed states with  $\xi_n^2 < 1$  because for such states  $4\langle\hat{J}_y^2\rangle > N$ , but, on the other hand, it deteriorates when  $\epsilon$  drops. These two effects more or less cancel each other for the parameters used in Fig. 2. However, for large  $N$ , the improvement coming from the quantum correlations dominates over the loss of signal, leading to the SSN scaling of the sensitivity.

Another distinguished time is when  $\phi = \frac{\pi}{2}$ . Then, the expression (24) simplifies to

$$\frac{\Delta\delta}{\delta} \geq \frac{1}{\sqrt{m}} \frac{1}{\epsilon} \frac{1}{\sqrt{4\langle\hat{J}_y^2\rangle + 4\langle\hat{J}_z^2\rangle}}. \quad (27)$$

Interestingly, in this case the sensitivity can be improved over the shot-noise scaling both for the phase-squeezed states, which give  $4\langle\hat{J}_z^2\rangle > N$ , or the number-squeezed states, which give  $4\langle\hat{J}_y^2\rangle > N$ . Still, the loss of the signal for small  $\epsilon$  can overshadow the SSN scaling, if  $N$  is not sufficiently large.

Finally, we focus on the long-time behavior of the QFI. When  $\varphi \gg 1$ , Equations (16) simplify and give a following bound for the sensitivity

$$\frac{\Delta\delta}{\delta} \geq \frac{1}{\sqrt{m}} \frac{\epsilon^2 + 1}{\theta\epsilon} \frac{1}{\sqrt{4\langle(\Delta\hat{J}_x)^2\rangle + 4\langle\hat{J}_z^2\rangle\epsilon^2}}. \quad (28)$$

If  $\epsilon \ll 1$  and the state is spin-squeezed with  $\xi_n^2 < 1$ , the  $4\langle\hat{J}_z^2\rangle\epsilon^2$  can be safely neglected, and we obtain

$$\frac{\Delta\delta}{\delta} \geq \frac{1}{\sqrt{m}} \frac{1}{\theta\epsilon} \frac{1}{\sqrt{4\langle(\Delta\hat{J}_x)^2\rangle}}. \quad (29)$$

If  $|\psi\rangle$  is strongly squeezed, i.e., close to the twin-Fock state  $|\psi\rangle \simeq |\frac{N}{2}, \frac{N}{2}\rangle$ , then  $\langle(\Delta\hat{J}_x)^2\rangle \simeq \langle\hat{J}_y^2\rangle$  and Equations (26) and (29) differ only by a presence of  $\epsilon$  in the denominator of the latter. Still, both expressions share the same scaling of the sensitivity with time. When  $\epsilon \simeq 1$  and  $|\psi\rangle$  is close to the coherent spin state or is phase-squeezed, then (28) is approximately

$$\frac{\Delta\delta}{\delta} \geq \frac{1}{\sqrt{m}} \frac{\epsilon^2 + 1}{\theta\epsilon^2} \frac{1}{\sqrt{4\langle\hat{J}_z^2\rangle}}. \quad (30)$$

This sensitivity breaks the SNL, scales inversely in time, and is only  $\frac{\epsilon^2 + 1}{\epsilon^2} \simeq 2$  times worse than the ultimate bound for the pure phase-imprint (10).

To summarize this Section, we have calculated the ultimate bound for the sensitivity of the double-well interferometer. We have shown, that it betrays the characteristic oscillatory behavior due to the presence of the Josephson term in the Hamiltonian (5). We have also shown that for some particular instants of time, the QFI can be improved beyond the SNL with either the number-squeezed or the phase-squeezed states. At long times and with spin-squeezed ( $\xi_n^2 < 1$ ) input states, the sensitivity closely resembles the precision of the MZI, whereas with phase-squeezed states ( $\xi_\phi^2 < 1$ ), it is almost as good as for a pure phase-imprint.

#### IV. ESTIMATION FROM THE POPULATION IMBALANCE

We now focus on a particular scheme of estimation based on the measurement of the population imbalance. The sequence we consider is following. First, the input state (8) evolves according to Eq. (7). Next, a population imbalance  $n$  between the two sites is measured. If this data is used to estimate the value of  $\delta$ , the CRLB reads

$$\Delta\delta \geq \frac{1}{\sqrt{m}} \frac{1}{\sqrt{F_{\text{imb}}}}. \quad (31)$$

Here,  $F_{\text{imb}}$  is the Fisher information for the population imbalance measurement. It is related to the conditional probability  $p(n|\delta)$  for detecting  $n$  given  $\delta$  as follows

$$F_{\text{imb}} = \sum_{n=0}^N \frac{1}{p(n|\delta)} \left( \frac{\partial p(n|\delta)}{\partial \delta} \right)^2. \quad (32)$$

The above probability results from the projection of the output state onto a state with  $n$  particles in one mode and  $N - n$  in the other

$$p(n|\delta) = |\langle n, N - n | \hat{U} | \psi \rangle|^2. \quad (33)$$

The Fisher information (32) through the CRLB (31) provides the maximal precision for the estimation of  $\delta$  from the population imbalance measurement, whichever estimator is used. Moreover,  $F_Q \geq F_{\text{imb}}$  always holds since the QFI sets the ultimate CRLB optimized over all the possible measurements.

Although the Fisher information from (32) is “the best you can get” from the population imbalance measurement, reaching the bound (31) requires the knowledge of the full probability (33). This renders the Fisher information approach impractical in most of the cases because in order to know (33) one must go through a laborious calibration stage. Therefore, typically some simpler estimators, which still utilize the data acquired from the measurements of the population imbalance, are used. The simplest estimator is based on the knowledge of the lowest moment of (33), namely the average, which is equal

to the mean of the population imbalance operator  $\hat{J}_z$

$$\langle n(t) \rangle = \sum_{n=-\frac{N}{2}}^{\frac{N}{2}} \binom{N}{n} p(n|\delta) = \langle \hat{J}_z(t) \rangle. \quad (34)$$

This average can be evaluated in the Heisenberg picture, where the  $\hat{J}_z$  reads

$$\hat{J}_z(t) = \hat{U}^\dagger \hat{J}_z \hat{U}. \quad (35)$$

Using the evolution operator (7), we obtain

$$\hat{J}_z(t) = u_x(t)\hat{J}_x + u_y(t)\hat{J}_y + u_z(t)\hat{J}_z. \quad (36)$$

The three time-dependent coefficients are

$$u_x(t) = \frac{\epsilon [\cos(\varphi\sqrt{\epsilon^2+1}) - 1]}{\epsilon^2 + 1} \quad (37a)$$

$$u_y(t) = -\frac{\sin(\varphi\sqrt{\epsilon^2+1})}{\sqrt{\epsilon^2+1}} \quad (37b)$$

$$u_z(t) = \frac{\cos(\varphi\sqrt{\epsilon^2+1}) + \epsilon^2}{\epsilon^2 + 1}. \quad (37c)$$

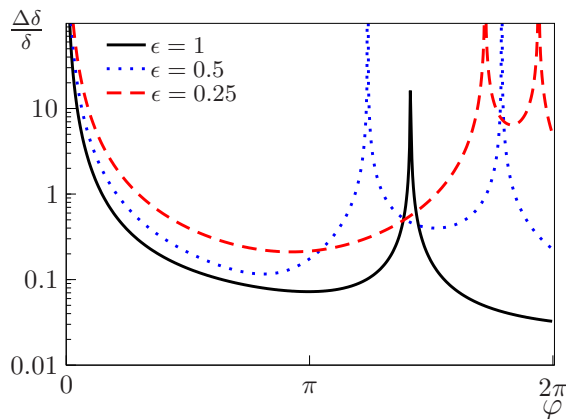


FIG. 4. (color online) The sensitivity  $\Delta\delta$  in units of  $\delta$  calculated using the error propagation formula for a spin-coherent state with  $N = 100$ . The Figure shows the Eq. (40) as a function of  $\varphi$  for three different values of  $\epsilon = 1$  (solid black line),  $\epsilon = 0.5$  (dotted blue line), and  $\epsilon = 0.25$  (dashed red line).

The scheme of the estimation from the average population imbalance is presented in [23, 28, 30]. First, we assume that the function (34) is known with  $\delta$  being a free parameter. In the experiment, this function is obtained in the calibration process. Then, the population imbalance is measured  $m$  times at time  $t$ . According to the central limit theorem, if  $m \gg 1$  the averaged outcomes are distributed with a Gaussian probability around the true mean value. This probability, together with the experimental outcomes, is used to construct the likelihood function  $\mathcal{L}(\delta)$ . In the final step,  $\delta$  is assigned to the value maximizing  $\mathcal{L}(\delta)$ . Such an estimator is unbiased and its

sensitivity is given by the error-propagation formula

$$\Delta\delta \geq \frac{1}{\sqrt{m}} \frac{\sqrt{\langle (\Delta\hat{J}_z(t))^2 \rangle}}{\left| \frac{\partial \langle \hat{J}_z(t) \rangle}{\partial \delta} \right|}. \quad (38)$$

The average and the variance of the population imbalance operator are expressed in terms of the two lowest moments of the angular momentum operators and the coefficients  $u_i$ . Combining Equations (36), (37), and (38), we obtain the bound for the sensitivity in units of  $\delta$

$$\frac{\Delta\delta}{\delta} \geq \frac{1}{\sqrt{m}} \frac{\sqrt{u_x^2(t)N \frac{\langle (\Delta\hat{J}_x)^2 \rangle}{\langle \hat{J}_x \rangle^2} + u_y^2(t)\xi_\phi^2 + u_z^2(t)\xi_n^2}}{\sqrt{N}\delta \left| \frac{\partial u_x(t)}{\partial \delta} \right|}. \quad (39)$$

It is again a complicated function of  $\epsilon$  and  $\varphi$ , and the input state. For a particular case of a spin-coherent state (18), when  $\xi_n^2 = \xi_\phi^2 = 1$ , we obtain that

$$\frac{\Delta\delta}{\delta} \geq \frac{1}{\sqrt{m}} \frac{\sqrt{u_y^2(t) + u_z^2(t)}}{\sqrt{N}\delta \left| \frac{\partial u_x(t)}{\partial \delta} \right|}. \quad (40)$$

We plot this result in Fig. 4 as a function of  $\varphi$  for the same three values of  $\epsilon$  as in Fig. 1. We observe similar behavior as in the case of the ultimate bound discussed in Section III. For each  $\epsilon$ , the sensitivity reveals some oscillatory features and the values of  $\Delta\delta/\delta$  are similar to those in Fig. 1. To complete the comparison, in Figures 5 and 6, we plot the expression (39) for the number-squeezed state ( $\xi_n^2 = 0.15$ ) and the phase-squeezed state ( $\xi_\phi^2 = 0.15$ ). Again, we observe the typical oscillatory behavior and quite similar values of the sensitivity.

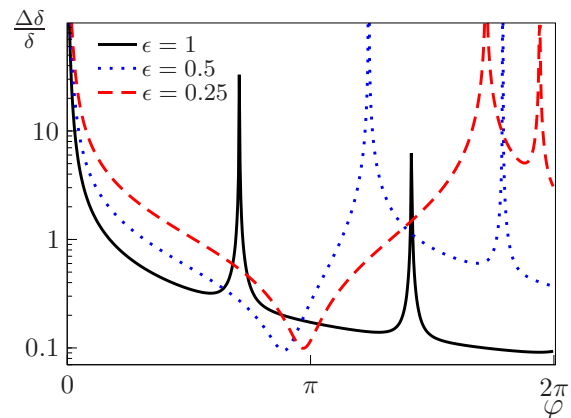


FIG. 5. (color online) The sensitivity in units of  $\delta$  calculated using the error propagation formula for a number-squeezed state of  $N = 100$  particles with  $\xi_n^2 = 0.15$ . The Figure shows the Eq. (39) as a function of  $\varphi$  for three different values of  $\epsilon = 1$  (solid black line),  $\epsilon = 0.5$  (dotted blue line), and  $\epsilon = 0.25$  (dashed red line).

In order to gain a better insight into the precision that can be achieved from Eq. (39), we again consider the

$\epsilon \ll 1$  and  $\varphi \simeq 1$  case. In this limit, we obtain that

$$\frac{\Delta\delta}{\delta} \geq \frac{1}{\sqrt{m}} \frac{1}{\sqrt{N}} \frac{1}{\epsilon} \frac{\sqrt{\xi_\phi^2 \sin^2 \varphi + \xi_n^2 \cos^2 \varphi}}{|\cos \varphi - 1|}. \quad (41)$$

To draw a parallel with the results from Section III, we first consider the case  $\varphi = \pi$  which simplifies Eq. (41) to

$$\frac{\Delta\delta}{\delta} \geq \frac{1}{\sqrt{m}} \frac{1}{\sqrt{N}} \frac{1}{2\epsilon} \xi_n. \quad (42)$$

This expression resembles the sensitivity of the estimation from the average population imbalance with the MZI

$$\frac{\Delta\delta_{\text{MZI}}}{\delta} \geq \frac{1}{\sqrt{m}} \frac{1}{\sqrt{N}} \frac{1}{\theta} \xi_n, \quad (43)$$

just as Eq. (25) resembles the ultimate bound of the MZI. Again, the ratio of those two is equal to  $\varphi/2$ . Nevertheless, the precision (42) improves below the SNL, if the interferometer is fed with a squeezed state with  $\xi_n^2 < 1$ .

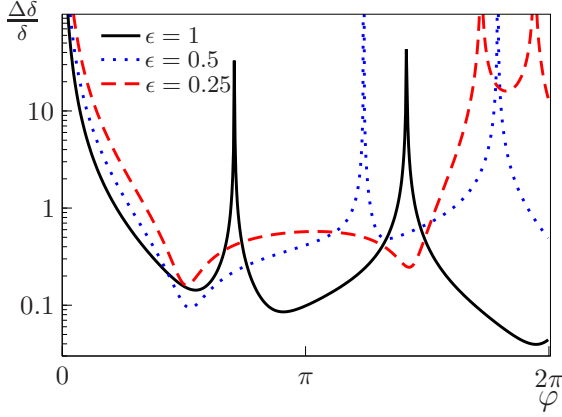


FIG. 6. (color online) The sensitivity  $\Delta\delta$  in units of  $\delta$  calculated using the error propagation formula for a phase-squeezed state of  $N = 100$  particles with  $\xi_\phi^2 = 0.15$ . The Figure shows Eq. (39) as a function of  $\varphi$  for three different values of  $\epsilon = 1$  (solid black line),  $\epsilon = 0.5$  (dotted blue line), and  $\epsilon = 0.25$  (dashed red line).

The other distinguished instant of time is when  $\phi = \frac{\pi}{2}$ . At this point, Eq. (41) transforms into

$$\frac{\Delta\delta}{\delta} \geq \frac{1}{\sqrt{m}} \frac{1}{\sqrt{N}} \frac{1}{\epsilon} \xi_\phi. \quad (44)$$

Again, there is a close analogy between this expression and the bound (27). As in the case of (27), the sensitivity (44) drops below the SNL, if the input state is phase-squeezed ( $\xi_\phi^2 < 1$ ). Note, however, that the presence of  $\epsilon$  in the denominator deteriorates the precision.

At long times, when  $\varphi \gg 1$ , and when  $\epsilon$  is small, the formula (41) takes an appealing form

$$\frac{\Delta\delta}{\delta} \geq \frac{1}{\sqrt{m}} \frac{1}{\sqrt{N}} \frac{1}{\theta\epsilon^2} \sqrt{\xi_\phi^2 + \xi_n^2 \cot^2 \varphi}. \quad (45)$$

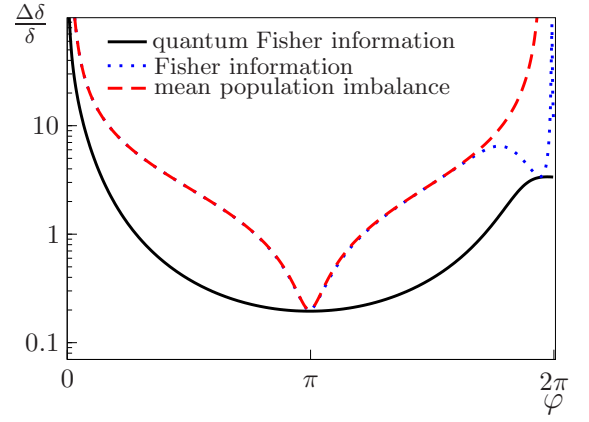


FIG. 7. (color online) Comparison of the three bounds for the estimation precision. The solid black line is the QFI from Eq. (12). The dotted blue line is obtained from the full population imbalance probability (31). The dashed red line is the error propagation formula for the estimation from the lowest moment of the population imbalance probability. The parameters are  $\epsilon = 0.1$ ,  $\xi_n^2 = 0.15$ , and  $N = 100$ .

Again, this expression scales inversely with time. At times such that  $\cot^2 \varphi = 0$ , this sensitivity, analogically to the short-time expression (44), breaks the SNL with phase-squeezed states. Nevertheless, the improvement from the particle entanglement might be eclipsed by the presence of  $\epsilon^2$  in the denominator.

Finally, we compare the ultimate sensitivity (12) with the Fisher information (31) and the error propagation information (39). In Fig. 7, we plot the sensitivity in units of  $\delta$  with  $\epsilon = 0.1$  as a function of  $\varphi$  for a spin squeezed state with  $\xi_n^2 = 0.15$ . We observe that the simple estimation from the average population imbalance gives the sensitivity almost as good as the Fisher information. Moreover, for  $\varphi = \pi$ , when Equations (25) and (42) hold, all the three methods give the same precision. This result can be explained as follows. At this time point, the sensitivities (25) and (42) resemble the precision of the MZI. For this interferometer, the Fisher information for the population imbalance probability (31) saturates the QFI for all states (8) with real coefficients  $C_n$  [34, 35]. A spin-squeezed ground state of the Hamiltonian (21) satisfies this condition, therefore, expressions (25) and (31) must coincide. On the other hand, such a state is Gaussian, meaning that it is characterized by the two lowest correlation functions. Not surprisingly, in such a case the sensitivity, which depends on these two moments (38), is as powerful as the estimation from the full probability (31). To summarize, at  $\varphi = \pi$  the simple estimation protocol from the average population imbalance is optimal, i.e., it saturates the ultimate bound of the QFI.

## V. CONCLUSIONS

We performed a systematic study of an atom interferometer which can be implemented in a double-well potential. This interferometer combines the phase imprint and the mode mixing at the same time. We derived the ultimate bounds for the precision of the parameter estimation and shown that these bounds improve from the particle entanglement of the spin-squeezed states. Importantly, for such an interferometer the estimation from the average population imbalance gives the sensitivity which closely resembles the expression obtained for the MZI. Finally, we have shown that this estimation method can be optimal at the half of the period of the Josephson oscillation. Such an oscillation-assisted interferometer, similarly to the Mach-Zehnder interferometer, can benefit from the time scaling of the sensitivity. However, in every limiting case, the precision of the interferome-

ter suffers from the loss of the signal, represented by the presence of  $\epsilon$  in the denominator.

Our work shows that a simple evolution operator (7) allows for an astonishing variety of interferometric scenarios, though the presented analysis is not general. We restricted our calculations only to pure states and assumed that the interactions are fully suppressed during the interferometric sequence. We did not take into account the impact of decoherence [36–38]. In any realistic application, the above theory should be extended to include those effects. Nevertheless, our results serve for two purposes. First, the idealized model tells what are the ultimate bounds for the precision of the parameter estimation. Second, these findings provide a simple theoretical background for a further analysis.

This work was supported by the National Science Center grant no. DEC-2011/03/D/ST2/00200.

- 
- [1] V. Giovannetti, S. Lloyd, and L. Maccone, *Science* **306**, 1330 (2004)
- [2] L. Pezzé and A. Smerzi, *Phys. Rev. Lett.* **102**, 100401 (2009)
- [3] A. Holevo, *Probabilistic and Statistical Aspects of Quantum Theory* (Scuola Normale Superiore, 2011)
- [4] M. Kitagawa and M. Ueda, *Phys. Rev. A* **47**, 5138 (1993)
- [5] D. Wineland, J. Bollinger, W. Itano, and D. Heinzen, *Phys. Rev. A* **50**, 67 (1994)
- [6] J. Esteve, C. Gross, A. Weller, S. Giovanazzi, and M. Oberthaler, *Nature* **455**, 1216 (2008)
- [7] J. Appel, P. J. Windpassinger, D. Oblak, U. B. Hoff, N. Kjærgaard, and E. S. Polzik, *P. Natl. A. Sci.* **106**, 10960 (2009)
- [8] C. Gross, T. Zibold, E. Nicklas, J. Esteve, and M. K. Oberthaler, *Nature* **464**, 1165 (2010)
- [9] M. F. Riedel, P. Böhi, Y. Li, T. W. Hänsch, A. Sinatra, and P. Treutlein, *Nature* **464**, 1170 (2010)
- [10] I. D. Leroux, M. H. Schleier-Smith, and V. Vuletić, *Phys. Rev. Lett.* **104**, 250801 (2010)
- [11] Z. Chen, J. G. Bohnet, S. R. Sankar, J. Dai, and J. K. Thompson, *Phys. Rev. Lett.* **106**, 133601 (2011)
- [12] T. Berrada, S. van Frank, R. Bücker, T. Schumm, J.-F. Schaff, and J. Schmiedmayer, *Nat. Commun.* **4** (2013)
- [13] B. Lücke, M. Scherer, J. Kruse, L. Pezzé, F. Deuretzbacher, P. Hyllus, J. Peise, W. Ertmer, J. Arlt, L. Santos, *et al.*, *Science* **334**, 773 (2011)
- [14] L. Pezzé and A. Smerzi, *Phys. Rev. A* **73**, 011801 (2006)
- [15] G. Ferrari, N. Poli, F. Sorrentino, and G. M. Tino, *Phys. Rev. Lett.* **97**, 060402 (2006)
- [16] N. Poli, F.-Y. Wang, M. G. Tarallo, A. Alberti, M. Prevedelli, and G. M. Tino, *Phys. Rev. Lett.* **106**, 038501 (2011)
- [17] M. Fattori, C. D’Errico, G. Roati, M. Zaccanti, M. Jonas-Lasinio, M. Modugno, M. Inguscio, and G. Modugno, *Phys. Rev. Lett.* **100**, 080405 (2008)
- [18] P. Cladé, E. De Mirandes, M. Cadoret, S. Guellati-Khélifa, C. Schwob, F. Nez, L. Julien, and F. Biraben, *Phys. Rev. Lett.* **96**, 033001 (2006)
- [19] I. Carusotto, L. Pitaevskii, S. Stringari, G. Modugno, and M. Inguscio, *Phys. Rev. Lett.* **95**, 093202 (2005)
- [20] R. Battesti, P. Cladé, S. Guellati-Khélifa, C. Schwob, B. Grémaud, F. Nez, L. Julien, and F. Biraben, *Phys. Rev. Lett.* **92**, 253001 (2004)
- [21] M. B. Dahan, E. Peik, J. Reichel, Y. Castin, and C. Salomon, *Phys. Rev. Lett.* **76**, 4508 (1996)
- [22] P. Cladé, arXiv:1405.2770
- [23] J. Chwedeńczuk, L. Pezzé, F. Piazza, and A. Smerzi, *Phys. Rev. A* **82**, 032104 (2010)
- [24] R. Gati, B. Hemmerling, J. Fölling, M. Albiez, and M. K. Oberthaler, *Phys. Rev. Lett.* **96**, 130404 (2006)
- [25] G.-B. Jo, Y. Shin, S. Will, T. Pasquini, M. Saba, W. Ketterle, D. Pritchard, M. Vengalattore, and M. Prentiss, *Phys. Rev. Lett.* **98**, 030407 (2007)
- [26] T. Schumm, S. Hofferberth, L. M. Andersson, S. Wildermuth, S. Groth, I. Bar-Joseph, J. Schmiedmayer, and P. Krüger, *Nat. Phys.* **1**, 57 (2005)
- [27] P. Böhi, M. F. Riedel, J. Hoffrogge, J. Reichel, T. W. Hänsch, and P. Treutlein, *Nat. Phys.* **5**, 592 (2009)
- [28] J. Chwedeńczuk, P. Hyllus, F. Piazza, and A. Smerzi, *New J. Phys.* **14**, 093001 (2012)
- [29] J. Grond, U. Hohenester, I. Mazets, and J. Schmiedmayer, *New J. Phys.* **12**, 065036 (2010)
- [30] J. Chwedeńczuk, F. Piazza, and A. Smerzi, *New J. Phys.* **13**, 065023 (2011)
- [31] H. Feshbach, *Ann. Phys.* **5**, 357 (1958)
- [32] C. J. Pethick and H. Smith, *Bose-Einstein Condensation in Dilute Gases* (Cambridge, 2008)
- [33] S. L. Braunstein and C. M. Caves, *Phys. Rev. Lett.* **72**, 3439 (1994)
- [34] T. Wasak, J. Chwedeńczuk, L. Pezzé, and A. Smerzi, arXiv:1310.2844
- [35] M. D. Lang and C. M. Caves, *Phys. Rev. Lett.* **111**, 173601 (2013)
- [36] R. Demkowicz-Dobrzański, J. Kołodyński, and M. Guta, *Nat. Commun.* **3**, 1063 (2012)
- [37] A. W. Chin, S. F. Huelga, and M. B. Plenio, *Phys. Rev. Lett.* **109**, 233601 (2012)
- [38] P. Szankowski, J. Chwedeńczuk, and M. Trippenbach, arXiv:1212.2528